Advancing Additive Manufacturing for Biomedical Applications: Antimicrobial and X-ray Absorptive Composite Filaments for Fused Filament Fabrication

A Thesis

Submitted to the Graduate Faculty of the
University of New Orleans
in partial fulfillment of the
requirements for the degree of

Master of Science in Engineering
in
Mechanical Engineering

by

John Arnold

B.S. University of New Orleans, 2018

December 2023

Dedication

This work is dedicated to the memories of my father and grandfather, John M. “Jack” Arnold Sr., and Marquis D. “Mark” Doyle Jr. No two men could possibly have been simultaneously so alike and so different. And no two men contributed more to the man I am today. I wish with all my heart that they could both have been here to see this. But I know they’re smiling with pride somewhere.

Acknowledgements

So many people have contributed to this work, and to my ability and motivation to complete it, that it would be impossible to include them all. I extend my deepest thanks to the following people, in no particular order:

To my grandmother, Constance F. “Connie” Doyle. For helping me find a way to continue my education, and for your support and encouragement. I couldn’t have done any of this without you and Pawpaw.

To my mother, Kay D. Arnold. For keeping the house full of books and instilling a love of learning, even though I mostly hated school. For never giving up on me, even when I gave up on myself. And for always seeing the man I could be, despite me being a little dumb sometimes. I can’t imagine how lost I might have been without such a great compass.

To my sister, Lauren L. Arnold. For being not only my constant cheerleader and biggest fan, but also an example and role model. Your dedication to your profession and your passion for education have inspired me more than you know. I’m sure you make an enormous difference in the lives of your students, but you’ve made an even bigger difference in mine.

To my wife, Stephanie Lassabe Arnold. For coming into my life at precisely the right moment and being so completely amazing. Your love inspires me to be better every day. Your kindness, patience, and positive energy make the hard parts easy. I am so happy we found each other, and I can’t wait to see all the amazing things the future holds for us.

To Dr. Damon A. Smith. For taking a chance on an eager but inexperienced undergraduate engineering student. So much of what I learned working on these studies makes its way into my work every day, I would not be the engineer I am today without it.

Contents

List of Figures

List of Tables

Abstract

The objective of this research was to investigate the use of nano- and microparticle amendments for the creation of Poly-lactic Acid composite materials for use in biomedical applications using the Fused Filament Fabrication process of Additive Manufacturing. Composites were created with the goal of imparting the useful properties of antimicrobial activity and x-ray absorption to the material. In addition to testing the efficacy of the particle amendments in achieving the desired properties, the thermal and mechanical properties of the composite materials were tested to ensure that the composites would be compatible with the Fused Filament Fabrication process and would produce a robust end product. In general, the sought-after properties were observed, while mechanical strength was reduced at high particle concentrations.

Keywords

Additive manufacturing, Biomedical devices, Biomedical phantoms, 3D printing, Fused filament fabrication, Fused deposition modeling, Thermoplastic composites, Antibacterial properties, Mechanical properties, Tensile testing, X-ray absorption

Introduction

Additive Manufacturing (AM) technologies, commonly referred to as 3d printing, are rapidly becoming a disruptive force in the manufacturing landscape. Advances over the past several years, both in the materials available for AM and in the 3d printers themselves, have brought what was once a niche method used mostly for prototyping to the forefront of modern manufacturing. Producers ranging from individuals to global companies are now employing AM to produce not only prototypes and models, but end use parts as well. AM is now being employed in industries where component performance is critical, such as aviation. GE, for example, utilized AM technology in their latest generation of turbines. Leveraging the ability of AM to create complex geometries allowed them to consolidate a fuel nozzle previously comprised of 20 individual parts into a single part which was lighter, more durable, and more efficient than the previous design (1). Boeing estimates they have over 70,000 3-d printed parts currently flying on various aircraft worldwide (2).

AM produces objects by building them up in finished or nearly finished form from raw material. This stands in contrast with more traditional manufacturing methods, such as machining (subtractive manufacturing), which produces finished parts by removing unneeded material from a solid block of material. AM offers several advantages over other manufacturing techniques, such as ease of customization and the ability to create complex geometries which would be difficult or impossible to achieve by other methods. Figure 3, below, shows the Fused Filament Fabrication (FFF) process of AM in progress, with annotations.

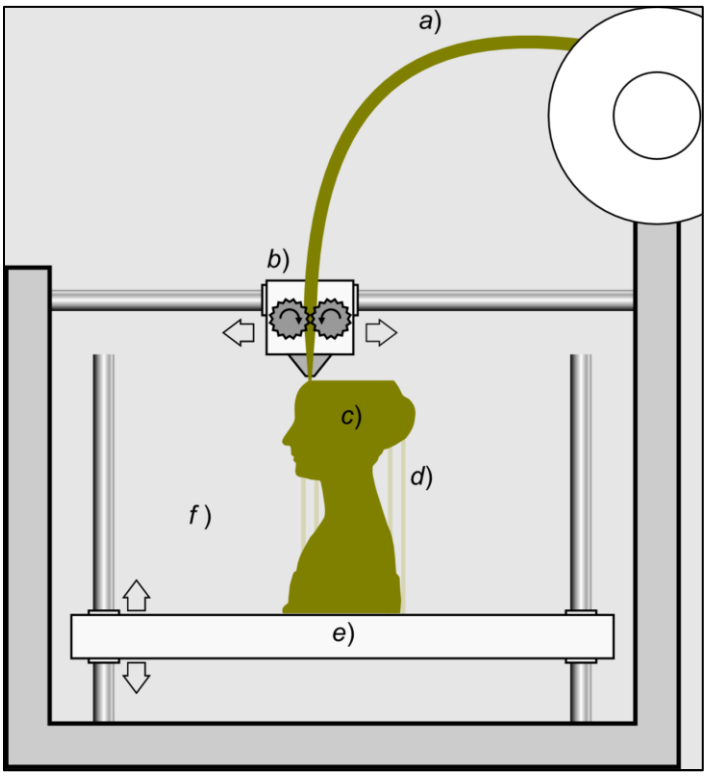

Figure 1: Schematic of FFF process showing a) incoming thermoplastic filament, b) print head with filament feed cogs and heated nozzle, c) the object being fabricated, d) supplemental support structures, and e) the print bed. (3)

FFF is the most commonly used AM process. This process utilizes a prepared thermoplastic filament fed through a heated nozzle. The nozzle heats the filament above its glass transition temperature which, along with the pressure exerted by the still solid filament being fed into the nozzle, extrudes a bead of molten thermoplastic from the nozzle orifice. The filament feed rate and motion of the nozzle are controlled by automation similar to that which is used in CNC machining, typically g-code, to produce objects of the desired shape. One layer of thermoplastic material is extruded and solidifies, then another layer is extruded on top of the previous layer. This process continues, building up the object in a stepwise manner until it is completed.

Poly-lactic Acid (PLA) is the most commonly used filament feedstock material for FFF. PLA is produced primarily from cornstarch and is readily biodegradable, making it more environmentally friendly than other thermoplastics which are typically derived from petrochemical sources. Biological sourcing also renders PLA very biocompatible, making it an excellent choice for medical applications. Environmental considerations, along with relatively low cost, make PLA a popular choice for AM as well as other production methods. Despite its advantages, PLA does have several potential drawbacks. It is more brittle, has lower tensile strength, and is less thermally stable than other common AM thermoplastics. PLA is also more hydroscopic than other AM polymers (4). This property can be either beneficial or detrimental, depending on the intended function and service life of the end product.

The research described in this thesis seeks to further advance the usefulness of AM by investigating particle additives which, when combined with the PLA polymer impart some new and useful property to the printed object. Such composites could be beneficial in a wide range of applications including biomedical devices, surgical tools, and environmentally friendly packaging.

Processing, Characterization, and Testing

The work detailed in this thesis is the product of two separate but similar studies investigating two distinct particle additives for use in PLA composites. A Silver sub-micron wire (Ag-SMW) additive was investigated due to the known antimicrobial properties of silver, as well as possible mechanical advantages due to the high aspect ratio of the particles. Bismuth Oxide (Bi_2O_3) powder was investigated for its known X-ray absorptive properties.

Due to the similarities between the two studies, much of the material processing, material characterization, and tensile testing work was performed using identical techniques and equipment. In the interest of brevity, this section describes the processes common to both studies along with any subtle differences. Processes which are either significantly different or unique to a particular study are detailed below in the section dedicated to the individual study.

Material Processing

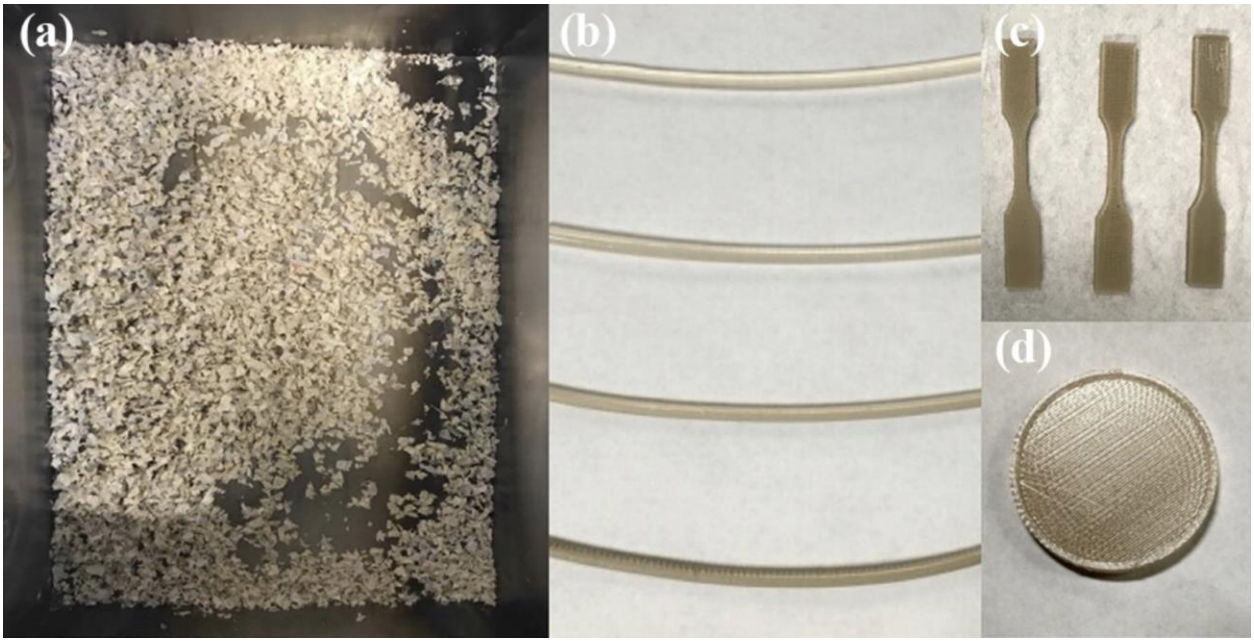

Figure 2: *(a) Composite granules used as feedstock for the extrusion of fused filament fabrication filaments; (b) extruded fused filament fabrication filaments containing (from top to bottom) 0.0, 0.1, 1.0 and 10.0 weight per cent of silver submicron-scale wire additives; (c) tensile; (d) antibacterial test specimens printed with composite filaments.*

Granule Production

Composite granules (Figure 2A) were prepared as feedstock for extrusion of FFF filaments for 3D printing test specimens. PLA pellets were added to chloroform and stirred vigorously at 50 °C until fully dissolved forming a 100 g/L solution. Particle additives were then added dropwise from a separate chloroform solution and stirred for two hours. The solution was removed from heat and allowed to dry under ambient

conditions for 48 hours. Residual solvent was removed from the dried composite in a vacuum oven at 50 °C for 24 hours. The composite was mechanically ground in a Dynisco Minigran granulator and passed through a 5 mm screen. The granulated composite was dried for an additional 24 hours under vacuum at 50 °C before use.

Filament Extrusion

Composite filaments (Figure 2B) were extruded using a single screw Filabot EX2 filament extruder. The composite granules were added to the system hopper and extruded at 180 °C at a rate of approximately 120-180 cm per minute. The composite was extruded through a 1.75 mm die. PLA filaments without additives were prepared with granules produced using the same procedures described above to exclude any variation of antibacterial, x-ray absorption, or mechanical testing results associated with the composite granule processing method.

Fabrication of Test Specimens

Specimens for both studies were produced using FFF. Nozzle and build platform temperatures were the same for both sets of specimens, 215°C and 60°C, respectively. 100% infill was used, and care was taken to ensure that the infill toolpath followed the long axis of the tensile specimens to maximize mechanical strength (5, 6, 7, 8). The specimens used in the AgSMW study were produced on a Fusion3 F400-S system with a glass bed, while the specimens for the Bi_2O_3 study were produced using a Prusa i3 MK3system with a polyetherimide bed. Due to performance differences between the two systems, the AgSMW specimens were produced using a print head speed of 70 mm/s, whereas the Bi_2O_3 specimens were produced using a print head speed of 50 mm/s for the perimeter and 200 mm/s for the interior. All specimens were held in a humidity-controlled cabinet at 20%RH for 24 hours prior to testing.

Material Characterization

Scanning Electron Microscopy

Particle morphology and fracture surfaces of tensile test specimens were observed using a Hitachi S-4800 scanning electron microscope at an accelerating voltage of 3 keV. Fracture surfaces were sputter coated with a 10 nm thick conductive gold film prior to imaging.

Differential Scanning Calorimetry

Differential scanning calorimetry (DSC) was performed using a TA Instruments SDT Q600 TGA-DSC in an Argon atmosphere. Samples were heated from 25°C to 250°C at a rate of 10°C/min. A single scan was

performed to obtain the glass transition temperature (T_G) and melting point (T_M) of each composite as a guide for extrusion and bed temperatures for FFF production of test specimens.

Tensile Testing

The mechanical properties of both composite materials studied were evaluated by tensile testing. While minor deviations were required due to the nature of the FFF process, tensile testing procedure was guided by the specifications for Type V specimens in ASTM D638-14. A typical tensile specimen used in these studies is shown below in Figure 3.

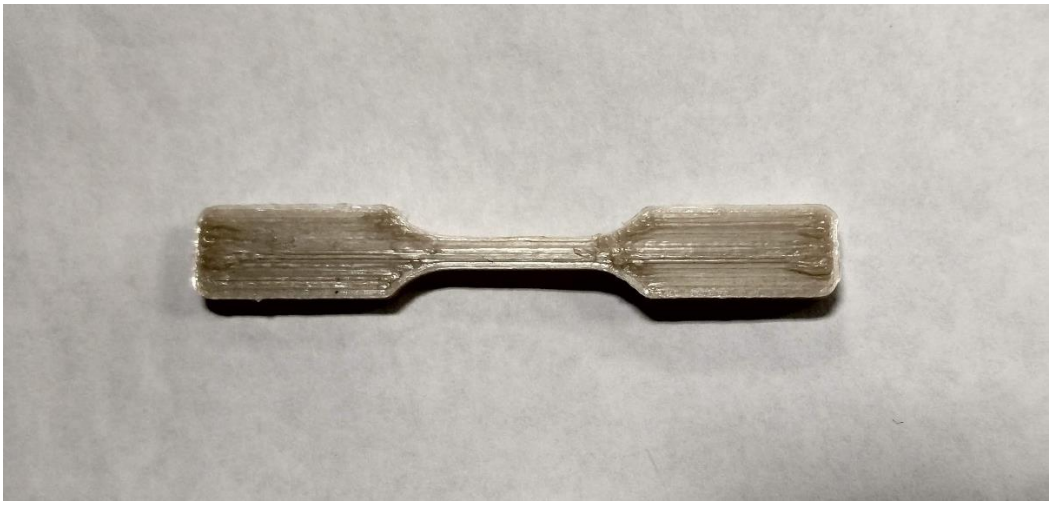

Figure 3: *Typical FFF produced tensile test specimen.*

Tensile testing was conducted at room temperature on an MTI Instruments SEMtester 2000 with a 9 kN load cell. Stress was applied at a rate of 6 mm/min with data collected at 10 Hz.

By analyzing the tensile test data, the ultimate strength, elastic modulus, and ductility of the composite specimens was determined.

Silver Sub-micron Wire Polylactic Acid Composite

Introduction

The geometric complexity and rapid customization achievable with additive AM have created a great deal of interest in the field of biomedicine (9, 10). Prosthetics, orthotics, splints, catheters, implants, and specialty surgical tools are just a few of the numerous applications being pursued using AM technologies as a new approach to customized health care (10, 11). In many of these applications it is important that the device be manufactured from a biocompatible material that is not prone to causing infections. Antibacterial materials are one of several approaches the United States health care industry is currently using to reduce the ~1.7 million hospital-acquired infections (HAIs) that patients experience annually (11, 12). These infections are often acquired by exposure to bacteria present on equipment and instruments (13). Therefore, there is a significant need for AM materials in emerging biomedical applications to possess both biocompatibility and antibacterial properties.

Though several AM technologies are employed for biomedical applications, FFF is the most popular process used due to the widespread availability of low-cost and reliable printing systems (14). Commercially available biocompatible filament options for FFF printers with antibacterial properties are currently limited and relatively few studies exist in the scientific literature on these materials.

One common approach to impart antibacterial properties to polymeric materials is through the incorporation of antibacterial metals. Silver, in particular, has been widely used for centuries for its antimicrobial properties. The metal releases silver ions, which have a strong cytotoxic effect on fungi, protozoa, several viruses, and both gram-positive and gram-negative bacteria (15, 16, 17). In this study, we investigate the use of silver particles as an antibacterial additive in polylactic acid (PLA) filaments for use with commercial FFF systems. PLA is the most common thermoplastic material used for biomedical applications due to its biocompatibility, biodegradability, mechanical properties, and its ease of processing (18). A wide variety of micro- and nanoscale additives have been previously explored as a means of modifying the properties of, or adding additional functionality to, thermoplastics (16, 18, 19, 20). We examine the use of high aspect ratio silver wires with diameters in the intermediate submicron range. While nanoparticle additives may exhibit novel properties attributed to their nanoscale dimensions or large surface-to-volume ratio, challenges related to processability and toxicity may exist in some materials systems (19, 21, 22). Therefore, we examine the use of submicron additives in an effort to reduce these challenges while still maintaining favorable surface interactions with the polymer matrix. We assess the use of this high aspect ratio additive for FFF printing of antibacterial objects and investigate the impact on the mechanical behavior of the material. To our knowledge, no current studies exist that investigate the antibacterial and mechanical properties of FFF-printed silver submicron wire (AgSMW) – PLA composites.

Experimental

Materials

Polylactic acid (PLA) polymer pellets (NatureWorks, 3D850) were purchased from Filabot (Barre, VT). Polyvinylpyrrolidone (PVP), silver nitrate (99.9999%), and anhydrous ethylene glycol (99.8%) were purchased from Sigma-Aldrich. Toluene, chloroform, Phosphate Buffered Saline (PBS), and BD Bacto tryptic soy broth were purchased from Fischer Scientific. Tryptic Soy Agar (TSA) CRITERION was purchased from Hardy Diagnostics. *Escherichia coli* (85W1660) was purchased from Ward Science.

Synthesis and Material Processing

Synthesis of Silver Micro-wires

AgSMWs with PVP coatings were produced in this study using the polyol synthesis method (23, 24). Ethylene glycol (50 mL) was heated to 60 °C in a reaction flask and degassed under vacuum for 4 hours using a Schlenk line. Two separate solutions of silver nitrate and PVP were prepared in 30 mL of ethylene glycol. These solutions were simultaneously injected with a syringe pump into the reaction flask heated to 160 °C under a nitrogen atmosphere at a rate of 375 µL per minute. The product was washed with toluene and collected by centrifugation at 5000 rpms for 15 min. The molar ratio of silver nitrate to PVP was prepared at 1.5 and the concentration of silver nitrate to the total ethylene glycol volume was 0.085 M.

Production, Fabrication, and Testing

Composite granule production, filament extrusion, and fabrication of test specimens were performed as described on pages 3 and 4 above. Figure 4, below, shows the AgSMW, PLA, and chloroform solution used to produce the composite granules. In this figure, the solution is fully mixed and prepared to be covered and set aside for drying at room temperature.

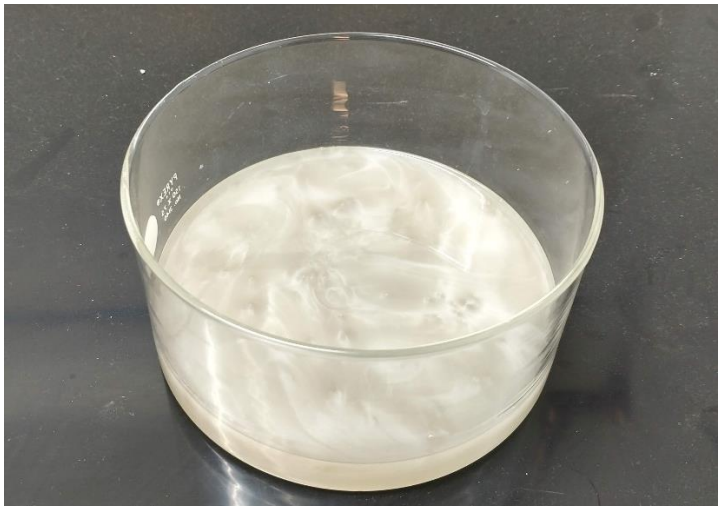

Figure 4: *AgSMW-PLA dissolved in Chloroform.*

Material Characterization

Microscopy, Calorimetry, and Tensile Testing

Electron microscopy, differential scanning calorimetry, and tensile testing were performed as described on page 4 above.

Antibacterial Testing

The antibacterial activities of test specimens were obtained against *Escherichia coli* (*E. coli*) strain 85W1660. E. coli was cultured in TSB at 37°C for 18-24 hours. The cultured bacteria were added to a 4mL 0.9% saline solution to reach approximately the concentration of 10^8 CFU/mL. A portion of the resulting solution was then further diluted to 10^6 CFU/mL. Four dishes 2.5 cm in diameter (Figure 2d) were fabricated using FFF, one for each of the three additive concentrations being tested and one control dish fabricated from pure PLA. The specimen dishes were placed into sterilized petri dishes and 500 µL of saline solution with cultured bacteria was added dropwise to the top surface of the test specimen. The samples were covered and left at room temperature for 24 hours. After 24 hours the test specimens were washed with 1mL of PBS each. 100µL of the resulting solution from each test sample was dispersed onto TSA culture medium. After incubation for 24 hours at 37°C, the surface area coverage of bacteria on the culture medium was measured using ImageJ image processing software.

Results and Discussion

Particle Morphology, Composite Processing, and Thermal Properties

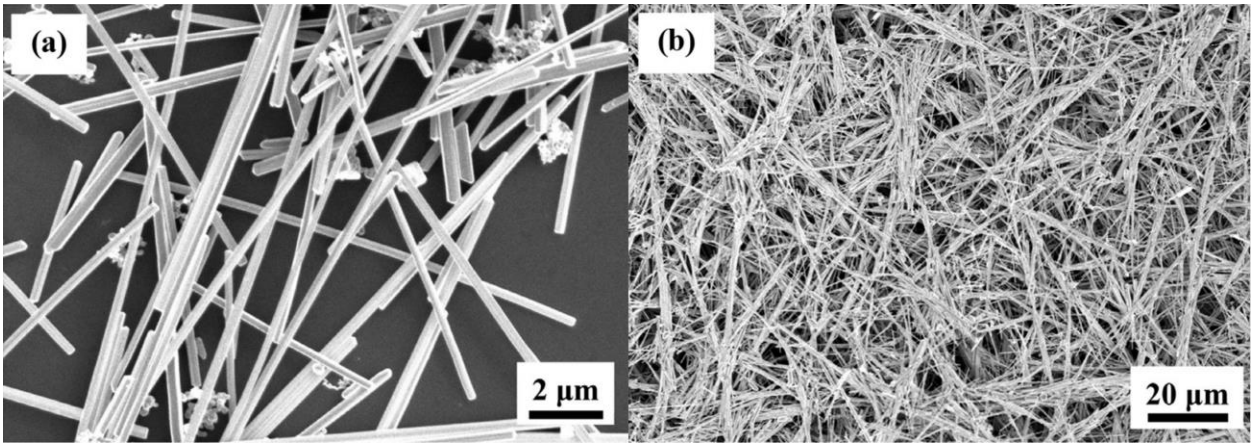

Figure 5: *Scanning electron microscopy images of polyvinylpyrrolidone coated silver submicron wires synthesized in this study.*

The molar ratio between PVP and AgNO3 in the polyol synthesis controls the morphology of the Ag particles (23, 24). SEM images (Figure 5) of the AgSMWs synthesized in this study display the characteristic faceted cross-section that results from anisotropic growth from dodecahedral seed particles containing multiple twin defects that are prevalent with low precursor concentrations (23). The wires had an average diameter of 0.330 mm 6 0.170 mm with an average aspect ratio larger than 20.

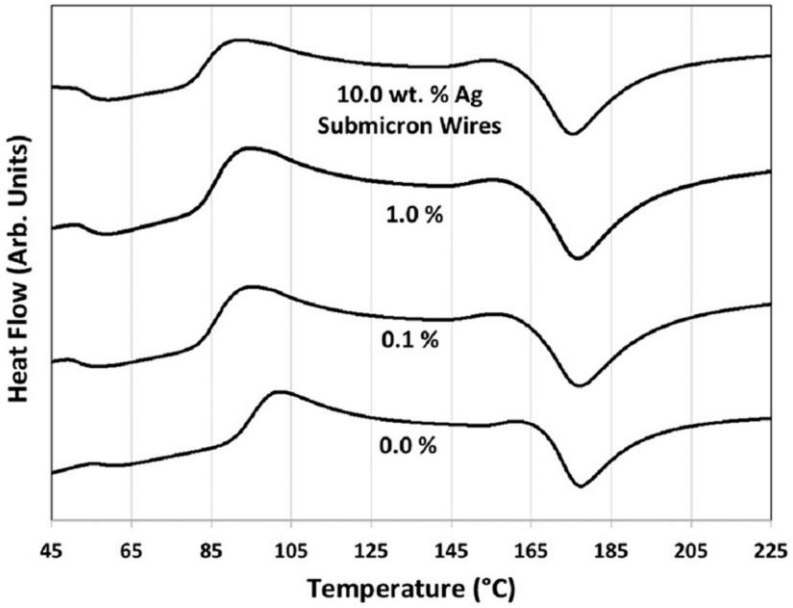

Figure 6: *Differential scanning calorimetry data for 0.0, 0.1, 1.0 and 10.0 weight percent of silver submicron wire additives in polylactic acid.*

Table 1: *Glass transition temperatures and melting points of composite filament granules containing varying concentrations of AgSMW*

AgSMW, wt%	T_G, °C	T_M, °C
0	57.3	177.4
0.1	52.0	177.0
1.0	53.8	175.4
10	53.8	175.4

DSC curves of the AgSMW composites are shown in Figure 6 compared to PLA containing no additives. The data indicate that the composite filaments produced have glass transition temperatures (T_G) and melting points (T_M) that do not vary significantly from the plain PLA filaments. Specific values extracted from the DSC curves are indicated in Table 1. This is consistent with observations of Ag nanowire-polymer composites in studies by Doganay et al. and Damm et al. The results indicate that no change is required for FFF process parameters for the composites studied.

Tensile Testing and Fractography

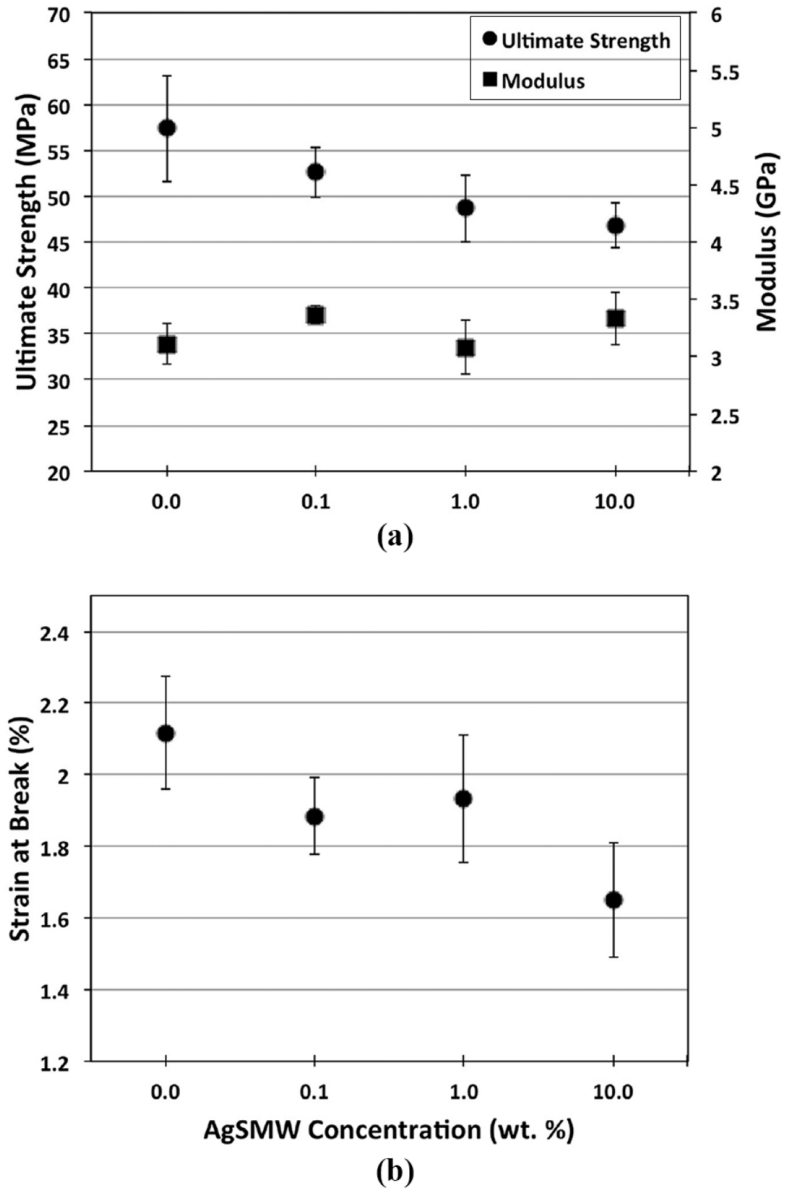

Figure 7: *(a) Ultimate strength, modulus; (b) strain at break versus silver submicron wire concentration for fused filament fabrication printed tensile test specimens.*

The ultimate tensile strength of the FFF-printed test specimens decreased moderately with increasing AgSMW concentration, while the elastic modulus did not change significantly (Figure 7a). The ductility of the test specimens, indicated by the strain at break displayed in Figure 7b, declines at the highest AgSMW concentration. The ductility of solvent processed PLA composites has been observed to increase in other studies because of residual solvent acting as a plasticizer at relatively low additive concentrations, which changes to brittle behavior at higher concentrations where the additive becomes dominant (19, 25, 26, 27). The lack of increased ductility indicated in this study suggests that the repeated drying steps described above sufficiently removes any residual solvent present in the composite mixture. Therefore, the decreased

ductility is likely a result of agglomeration or an increase in defect density because of poor additive-polymer interfacial interactions at high additive concentrations. The PVP coating on the AgSMWs allows for good dispersibility in the chloroform solution, but no significant interaction is expected between the PVP coating and PLA. Poor interfacial adhesion would also explain the observed trend of decreasing ultimate tensile strength with increasing AgSMW concentration and the lack of any significant change displayed by the elastic modulus.

SEM images of the fracture surfaces of FFF-printed test specimens fractured under tensile load, shown in figures 8 and 9 below, provide further insight into the mechanical behavior observed.

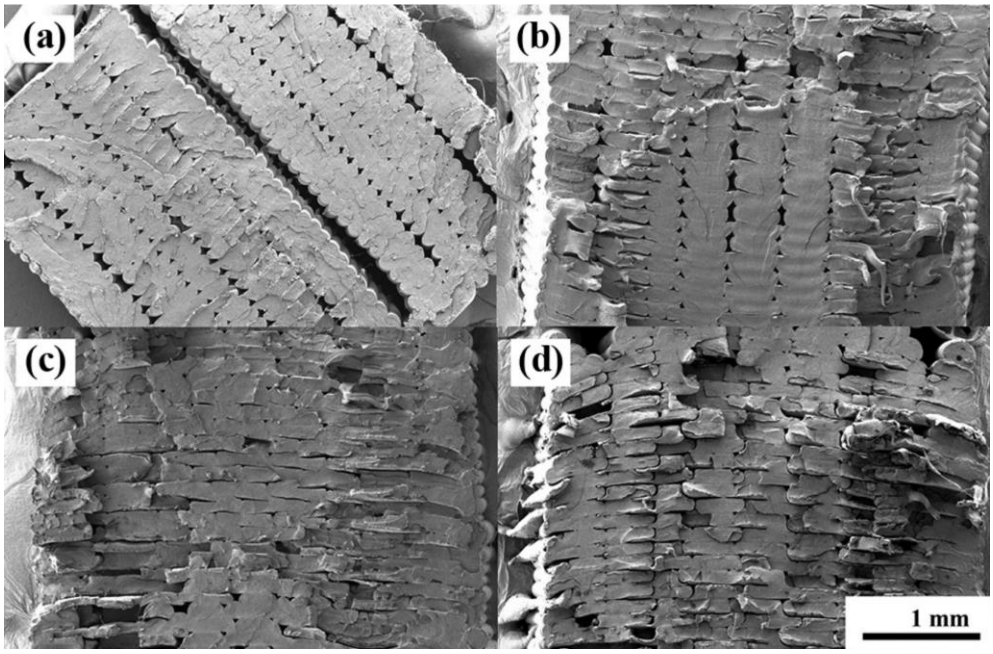

Figure 8: *Scanning electron microscopy images of representative tensile specimen fracture surfaces from (a) polylactic acid; (b) 0.1; (c) 1.0; (d) 10.0 weight per cent silver submicron-scale wire additives in polylactic acid.*

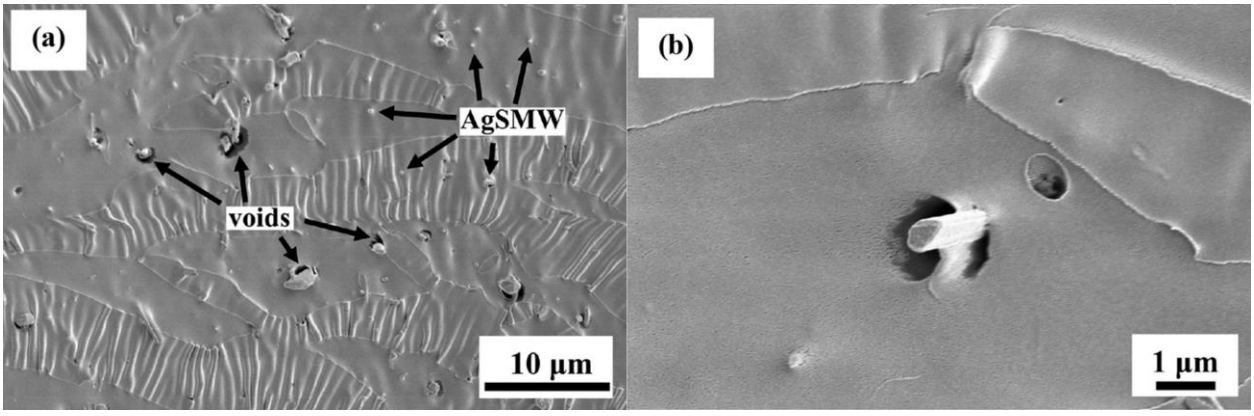

Figure 9: *Scanning electron microscopy images of representative tensile fracture surface showing (a) silver submicron-scale wire distribution and void defects and (b) detail showing an individual wire exhibiting pull-out behavior upon fracture and surrounding void.*

Figure 8 shows the presence of flat planes indicative of brittle fracture commonly observed for semi-crystalline polymers (28). The fracture surfaces also show AgSMWs largely aligned perpendicular to the surface [Figure 9(a)] indicating a preferential alignment because of shear forces present in the extrusion head of the printing system. Void defects are also observed between the AgSMWs and the PLA matrix throughout the specimens, indicative of poor bonding between the additive and polymer matrix. This is further indicated by the presence of wires jutting out above the fracture surface (Figure 9) denoting pull-out behavior associated with the lack of significant interfacial bonding. No obvious agglomeration of additives was observed on fracture surfaces; therefore, the addition of the large density of void defects within the specimen is the likely reason for the reduced strength and ductility. The specimen cross-sections display a microstructure with interstitial voids between the deposited filaments and stacked layers that is the characteristic of FFF-printed objects (14). A reduction of interstitial void size can be observed in the representative fracture surfaces in Figure 8 as the additive concentration increases.

The shape of deposited beads and resulting void size in the FFF process is a result of several factors including the viscosity of the melted material, the print surface, and interactions between the print nozzle and the bead (14, 29, 30). Notably, Costa et al. showed that a reduced viscosity led to greater coalescence and adhesion between extruded filaments. The presence of nanoparticles in a polymer matrix can dramatically reduce the viscosity of a composite (31). Therefore, it is likely that the viscosity of the melt is reduced with increasing AgSMW additive concentration, but the details of this phenomenon are left to future studies. Despite the greater infill observed at higher additive concentrations, the ultimate strength and ductility are still reduced indicating that the increased contact area between deposited filaments does not play a dominant role in determining the mechanical behavior analyzed in this study.

Antibacterial Testing

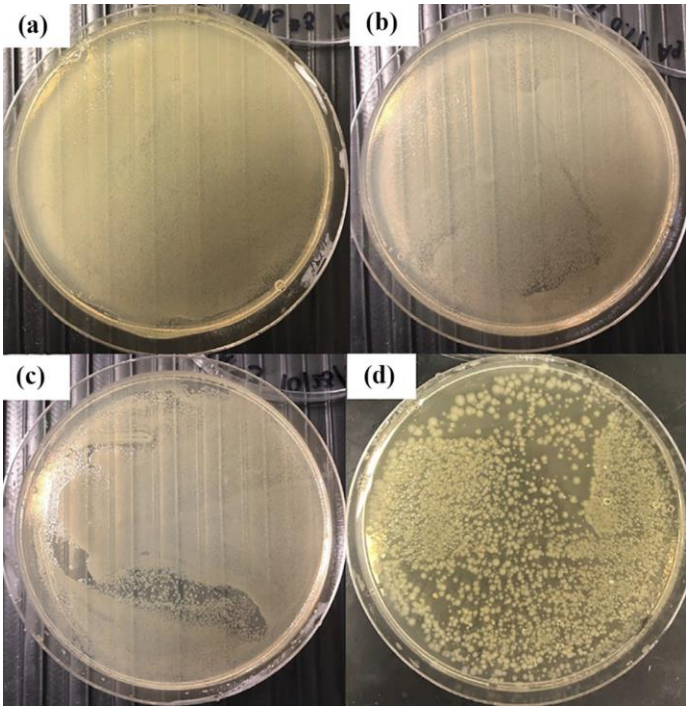

Figure 10: *Representative samples of surviving E. coli colonies after exposure to (a) polylactic acid; (b) 0.1; (c) 1.0; (d) 10.0 weight per cent silver submicron-scale wire-polylactic acid composites*

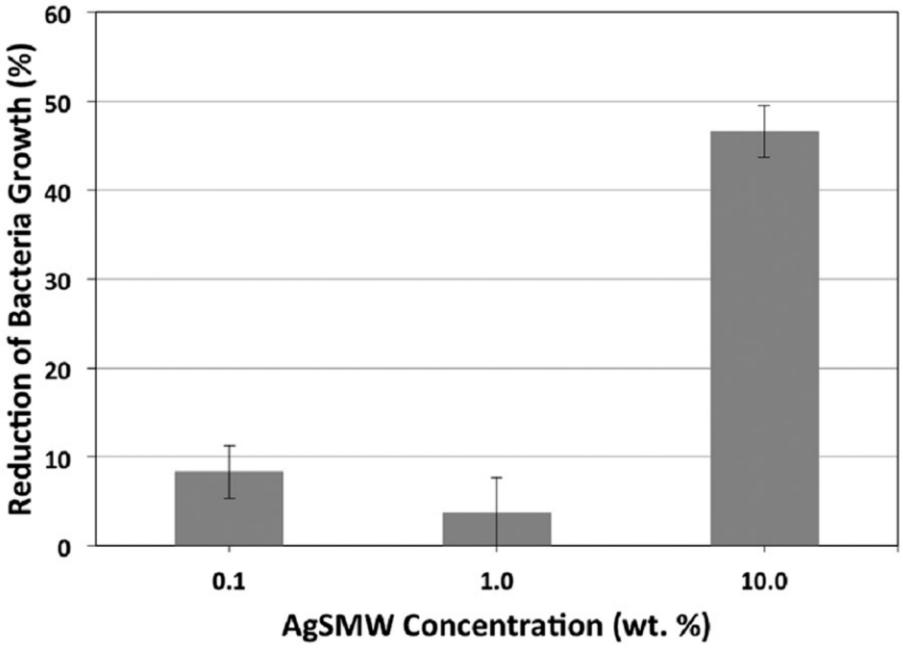

Figure 11: *Reduction of E. coli growth versus silver submicron-scale wire concentration*

The results of the antibacterial testing against E. coli are shown in Figures 10 and 11 above. A negligible reduction in bacteria growth is observed for 0.1 and 1.0 weight per cent concentrations. However, significant antimicrobial activity is observed at the 10.0 weight per cent AgSMW concentration with a reduction in growth close to 50 per cent. Silver ion release from the composite is the primary mechanism for the reduction of bacteria growth (15, 17). Bacteria likely make some direct contact with Ag additives located on the surface of the composite, but ions are expected to reach the bacteria primarily through the diffusion of water into the bulk of the polymer matrix (16, 32, 33, 34). Therefore, both the choice of polymer matrix for antibacterial metal composites and its associated rate of water diffusion have a significant impact on the additive concentration required. Based on reported values of the water diffusion coefficient of PLA, it is expected that water would penetrate to a depth of approximately 300 mm over the 24-hour period that the E. coli containing droplets are in contact with the composite surface (35). While only a relatively shallow penetration of water into the bulk polymer is expected, the presence of void defects observed in the microstructure around the AgSMW may also facilitate ion release.

Conclusions

AgSMWs were assessed as an antimicrobial additive in PLA for biomedical applications. The silver additives were synthesized with a PVP coating and processed with PLA to form composite granules using solvent processing and granulation. Composite granules with AgSMW concentrations from 0.1 to 10 weight percent were used to extrude filaments that were compatible as feedstock for commercial FFF printing systems. The thermal properties of the composites were relatively unchanged by incorporation of AgSMWs, allowing the printing of test specimens using print settings identical to those used for pure PLA.

A strong antibacterial effect was observed against E. coli at an additive concentration of 10 weight percent. The reduction of bacteria growth is attributed to the release of silver ions facilitated by penetration of water in the bulk composite, both by diffusion and by penetration into voids observed in the microstructure.

The impact of the addition of PVP-coated AgSMWs on the tensile mechanical properties of the composite material was also considered. The strain at break of the FFF produced test specimens was reduced at the highest particle concentration. The ultimate tensile strength decreased with increasing particle concentration. The elastic modulus of the composite material was not significantly different from that of pure PLA control. Reduced strength and ductility are attributed to void defects observed between the AgSMW particles and the polymer matrix.

The results indicated in this study demonstrate the efficacy of using antibacterial AgSMW PLA composites for FFF printing. Although a slight degradation of mechanical properties is observed, particularly at the highest concentration, the composite has potential for a wide variety of biomedical applications.

Bismuth Oxide Poly-lactic Acid Composite

Introduction

The rapid emergence of AM has created exciting opportunities for medical education, patient engagement, and clinical care delivery (36, 37, 38). AM provides a quick and economical means to produce objects with complex geometries that can address patient-specific needs. Applications include prosthetics (10, 39), anatomical models for surgical planning (40, 41), and education (42-47). The ability of AM to produce highly customized anatomical models that can not only be visualized but also manipulated in three dimensions by touch has shown promise as a valuable tool in diverse medical fields ranging from neurosurgery (48, 49), orthopedics (50,51), otolaryngology (52), and cardiothoracic surgery (53). These devices and models can often be printed directly from, or in concert with, computed tomography (CT) images of patient anatomy (54). An important material consideration in many of these applications is the opacity of the printed objects when imaged by medical X-ray systems, such as CT, radiography, and fluoroscopy. This radiopacity needs to be relatively high for surgical tools and implants so that they can be easily identified. For biomedical phantoms, however, the material should mimic the radiographic characteristics of the anatomical features being modeled. Relatively few studies currently exist in the literature which explore the use AM materials with controlled radiopacity for biomedical phantom applications, providing the primary motivation for the work described in this study (55, 56).

Commercially available FFF filaments have relatively low radiopacities when compared to certain anatomical features, limiting their applicability for many phantom applications. One common approach to impart an increased radiopacity to polymeric materials is through the incorporation of radiocontrast agents that possess high X-ray attenuation coefficients (57). Typical additives are dense powders containing elements with high atomic numbers and K-shell binding energies (K-edge) that are comparable to the energy spectrum of the medical imaging system. Some of the most common powders used are barium sulfate, tungsten, and bismuth compounds (57, 58). Of these additives, bismuth compounds, such as bismuth oxide (Bi_2O_3) offer some distinct advantages. It has a higher density and K-edge than bismuth sulfate, providing a greater radiopacity at lower loadings. While tungsten has a higher density than Bi_2O_3, its use in an extrusion-based AM process can cause much greater abrasive wear on the extrusion head of FFF printers (14). In this study we investigate the use of Bi_2O_3 microparticles in polylactic acid (PLA) filaments for FFF printing of a biomedical spine phantom for CT imaging. Microcomputed tomography (micro-CT) is used to image the microparticle distribution within the printed objects and to calibrate the composite concentration to mimic the CT contrast of bone. In addition, we assess any mechanical degradation of the printed composites due to the additive that might affect their applicability in load-bearing applications.

Materials and Methods

Materials

PLA polymer pellets (NatureWorks, 3D850) were purchased from Filabot (Barre, VT). Bi2O3 powder (99.9%, 10 μm diameter) and chloroform were purchased from Sigma–Aldrich and Fischer Scientific, respectively.

Material Processing

Production, Extrusion, and Fabrication

Composite granule production, filament extrusion, and fabrication of test specimens performed as described on pages 3 and 4 above. Shown below in Figure 12 are representative the test specimens fabricated for this study.

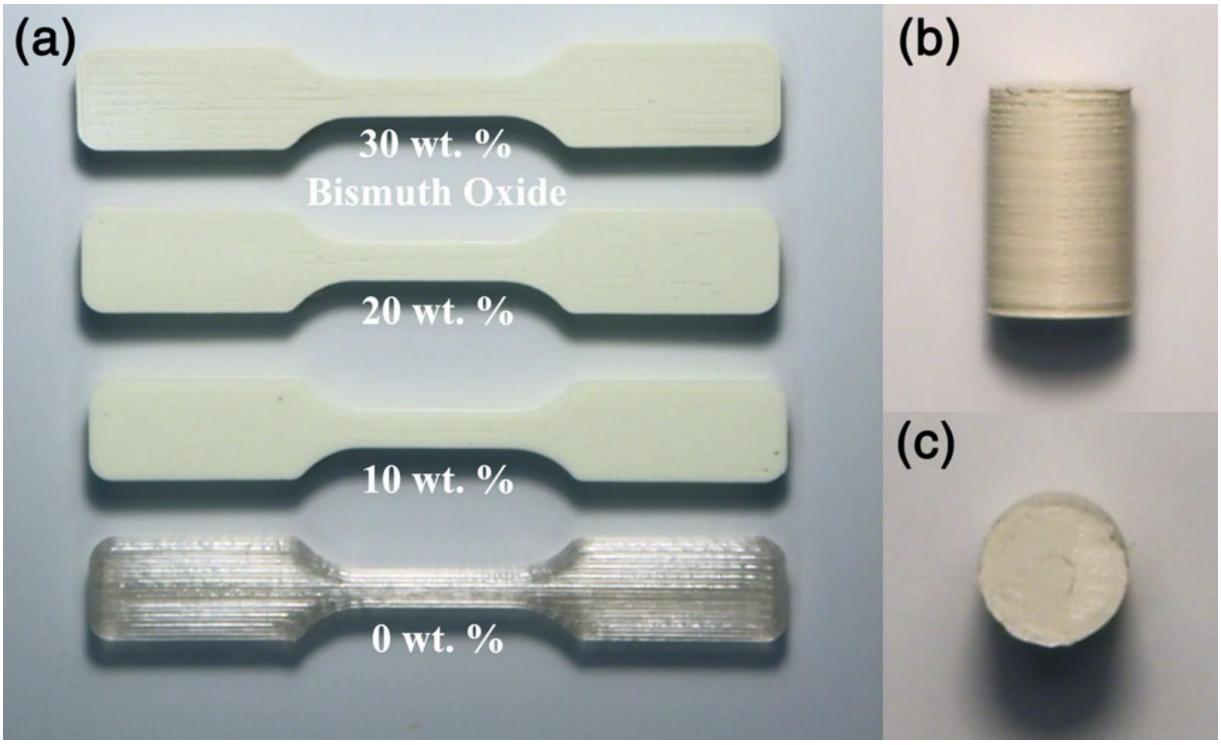

Figure 12: *a) FFF printed PLA tensile test specimens containing 0, 10, 20, and 30 wt% bismuth oxide particles. (b) Side and (c) top view of a representative cylindrical PLA test specimen containing 30 wt% bismuth oxide particles for microcomputed tomography analysis.*

Development and Fabrication of Spine Phantoms

Phantom models were created and printed based on CT of the cervical spine without contrast C2-T1. This imaging was taken from a patient who received neurological and neurosurgical care at Ochsner Health. The CT scan was obtained in the process of routine care and surgical evaluation. The patient has a history of Neurofibromatosis Type 1 with previous C2/C3 anterior cervical discectomy and fusion with cervical

kyphotic deformity. The patient presented with debilitating neck pain, arm weakness and progressive cervical myelopathy and underwent second stage anterior stabilization and instrumented fusion. The Digital Imaging and Communication in Medicine (DICOM) data were procured, segmented, and printed with an Ochsner IRB approved protocol (2017.066A).

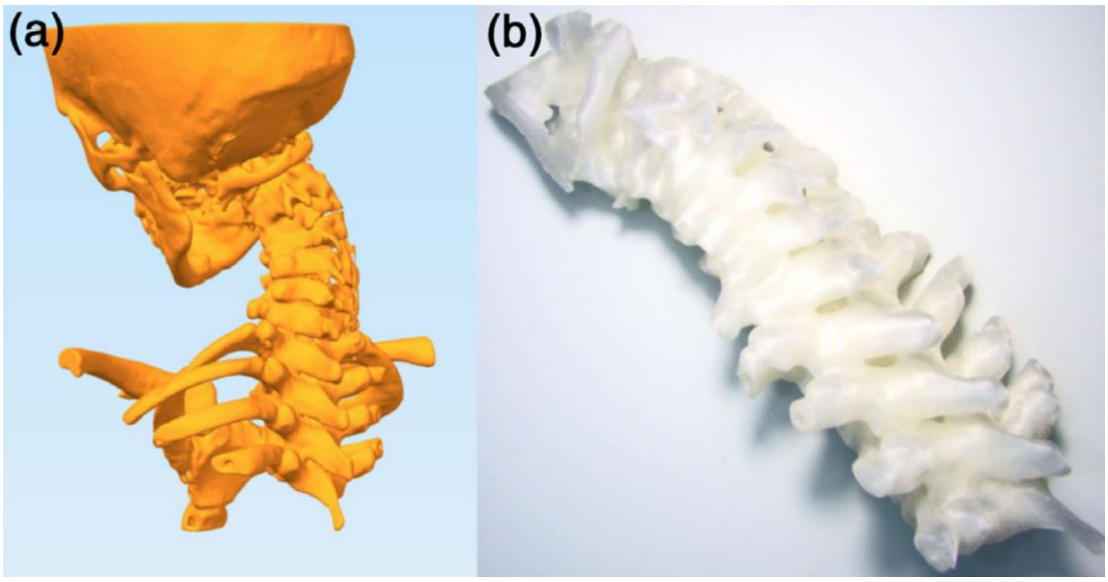

Figure 13: *a) 3D stereolithography model and a (b) representative PLA FFF print of a phantom developed from a computed tomography image of a patient with a history of Neurofibromatosis Type 1 with previous C2/C3 anterior cervical discectomy and fusion with cervical kyphotic deformity*.

3D Slicer, an open-source software, was used to segment the DICOM data and create the STL model shown in Figure 13a. Figure 13b shows a representative FFF print of the spine portion of the model using PLA as the build material. The same print temperatures and speeds were used as indicated in *Fabrication of Test Specimens*, on page 4. While a 100% rectilinear interior infill setting was also used to print the models, 10 perimeters and 10 solid top and bottom layers were used with a concentric infill pattern to improve the overall surface finish of the highly curved outer geometry. For CT testing, vertebral bodies were extracted from the STL model shown in Figure 13a and printed with PLA and a 1.5 wt% bismuth oxide-PLA composite filament. Phantoms were also stored in a humidity-controlled cabinet at 20% RH for 24 hours prior to testing with no additional post-processing.

Material Characterization

Microscopy, Calorimetry, and Tensile Testing

Electron microscopy, differential scanning calorimetry, and tensile testing were performed as described on page 4 above.

X-ray Microcomputed Tomography

Micro-CT images were acquired on an Xradia microXCT 400 scanner. A 5 mm diameter by 5 mm length cylindrical volume was scanned from the interior region of each of the test specimens and calibration samples using identical beam and reconstruction parameters. The calibration standards were scanned empty and filled with deionized (DI) water. The scans were taken using a 4X objective at 120 kV, a power of 10 W, and a 3.5 second acquisition time. Images were reconstructed with an isotropic resolution of 5.5 μm. The average CT number of the specimens in Hounsfield units (HU) was determined using a linear calibration based on the measured average 16-bit grayscale values of the micro-CT images of air and water and their known CT numbers of −1,000 and 0 HU, respectively (56,59). CT images of the spine phantoms were acquired on a GE Lightspeed VCT 64 Slice scanner with a resolution of 0.625 mm. Image analysis was performed using the imageJ open-source software.

Results and Discussion

Thermal Analysis

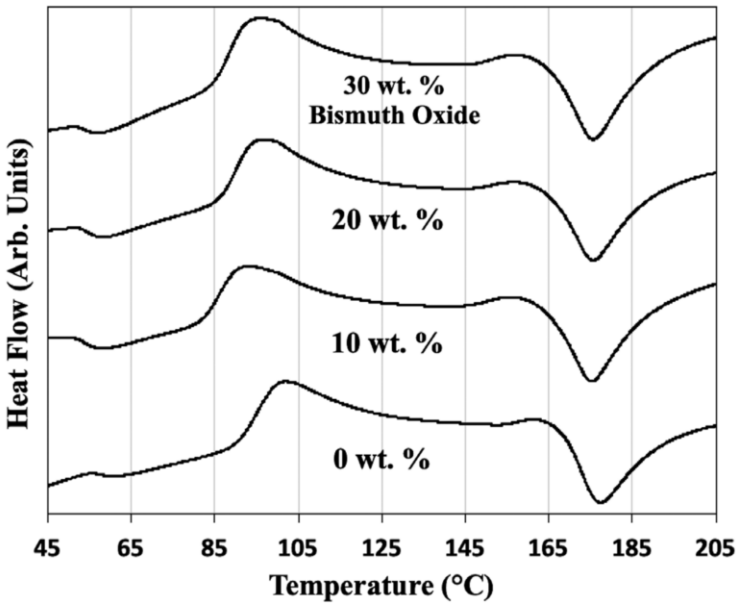

Figure 14: *Differential scanning calorimetry data for bismuth oxide composite granules produced with varying concentrations used to produce filaments for fused filament fabrication (FFF) printing systems.*

Table 2: *Glass transition temperature and melting point of composite filament granules containing varying concentrations of Bi_2O_3*

Bi_2O_3, wt%	T_G, °C	T_M, °C
0	58.2	177.4
10	55.2	175.2
20	55.7	175.6
30	54.6	175.7

DSC curves of the Bi_2O_3-PLA composite granules processed using the methods described above are shown in Figure 14 compared to PLA containing no additives. Analysis of the DSC data shown in Table 2 indicates that the composites produced have a T_G and T_M that dropped only slightly compared to PLA produced with no additives.

Mechanical Properties and Fractography

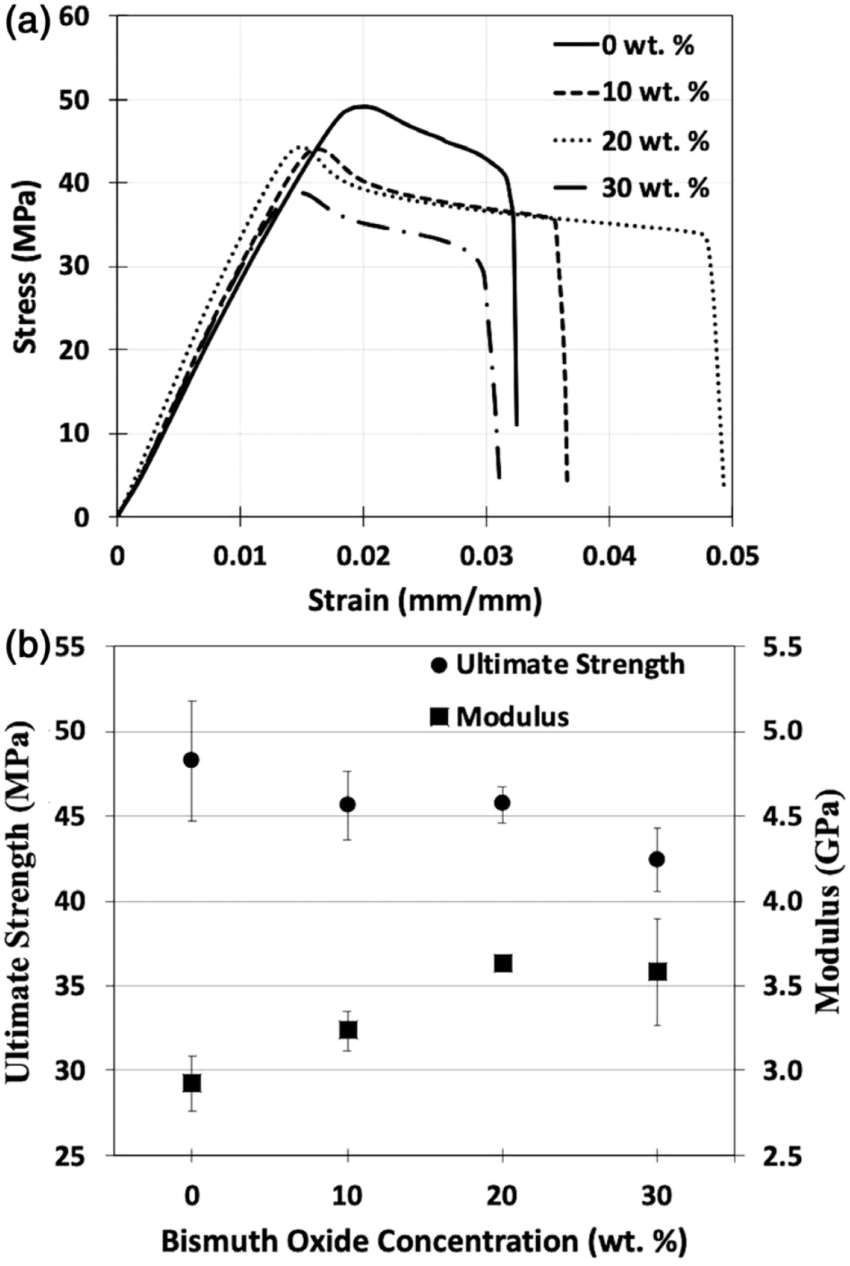

Figure 15: *a) Representative stress–strain curves and (b) the average ultimate strength and modulus of FFF printed PLA tensile test specimens with varying concentrations of bismuth oxide*.

Figure 15a shows representative stress–strain curves for each of the Bi_2O_3 concentrations studied. Analysis by one-way ANOVA showed a statistically significant change in both the ultimate strength ($F(3, 16) = 5.287$, $p = 0.01$) and modulus ($F(3, 27) = 15.946$, $p = 5e\text{-}5$). The average ultimate strength and modulus of the test specimens for each concentration are shown in Figure 15b. Post hoc comparisons using a t test with Bonferroni correction showed that there was no significant change in the ultimate strength of the concentrations. studied below 30 wt%. The average ultimate strength of the specimens containing 0, 10, 20, and 30 wt% concentrations were 48.2 ± 3.6, 45.6 ± 2.0, 45.7 ± 1.0, and 42.4 ± 1.9 MPa, respectively. At the highest additive concentration of 30 wt% the average ultimate strength was reduced by 12% compared to plain PLA specimens. The change in modulus was significant for each concentration studied compared to plain PLA. The average modulus of specimens containing 0, 10, 20, and 30 wt% concentrations were 2.92 ± 0.16, 3.23 ± 0.11, 3.64 ± 0.04, and 3.58 ± 0.31 GPa, respectively. The average modulus of the specimens was found to increase with the addition of Bi_2O_3 with a maximum increase of 24% compared to plain PLA specimens.

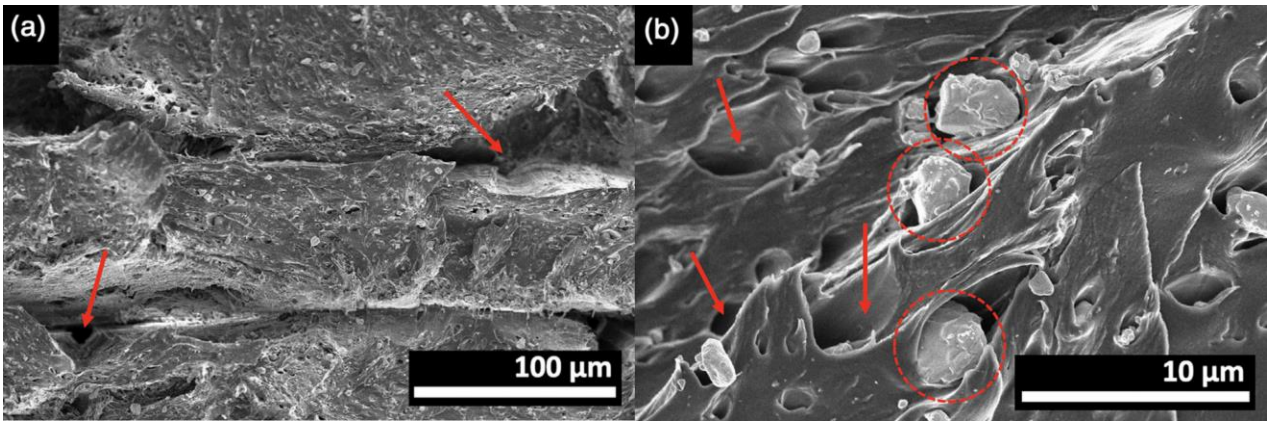

Figure 16: *a) Low-magnification (400×) SEM image of a representative fracture surface of an FFF printed tensile test specimen containing 30 wt% bismuth oxide. Interstitial voids (indicated by red arrows) can be observed between the layers of the deposited composite. (b) High-magnification (4500×) SEM image showing the presence of bismuth oxide particles embedded in the PLA (indicated by red arrows). Micron-scale voids (indicated by dashed circles) are also displayed throughout the surfaces resulting from pull-out upon fracture.*

Figure 16 shows SEM images of the fracture surface of a representative FFF printed test specimen containing 30 wt% Bi_2O_3. The specimens display a number of notable features. Overall, the fracture surfaces show flat planes with interstitial voids (Figure 16a) between the deposited composite material. The distribution of the Bi_2O_3 can also be observed in the high-magnification SEM image (Figure 16b) with an average diameter of 1.28 ± 0.95 µm based on a random sampling of >100 particles. The additives were distributed homogeneously throughout the PLA matrix with some noticeable particle agglomeration observed. In addition, micron-scale voids can be seen in Figure 16b along the entire flat fracture surfaces of the PLA.

Computed Tomography Analysis

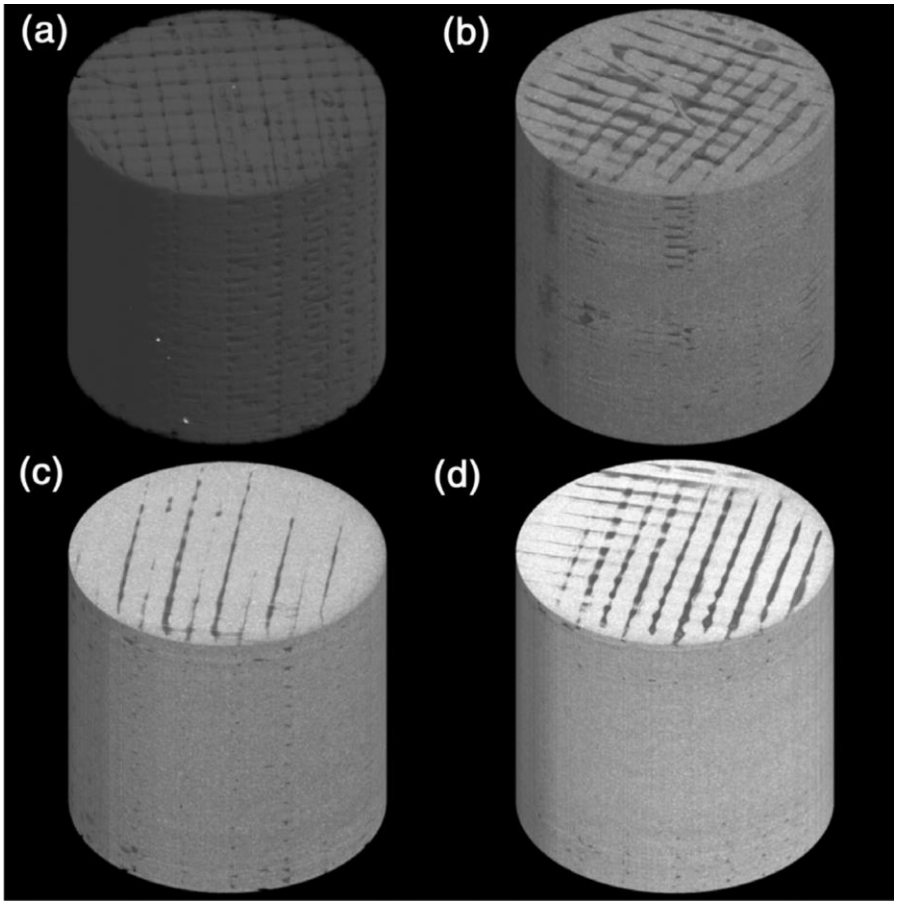

Figure 17: *3D microcomputed tomography (micro-CT) images of FFF printed specimens containing (a) 0, (b) 10, (c) 20, and (d) 30 wt% bismuth oxide showing an increase in 16-bit grayscale values with increasing bismuth oxide concentration.*

3D micro-CT images of the interior of the cylindrical test specimens with varying Bi_2O_3 concentrations are shown in Figure 17. The micro-CT images show that the specimens had some regions with infills significantly below 100%. Image analysis of the filled and unfilled regions of the volume showed that the reduced infill resulted in an overall average porosity of 9 ± 4%. The average contrast represented by 16-bit grayscale values in the micro-CT images is observed to increase with increasing Bi_2O_3 content in Figure 17. The images show that the composite has a grainy appearance throughout the solid regions, indicative of the existence of particle clusters observable within the 5.5 μm resolution of the micro-CT image.

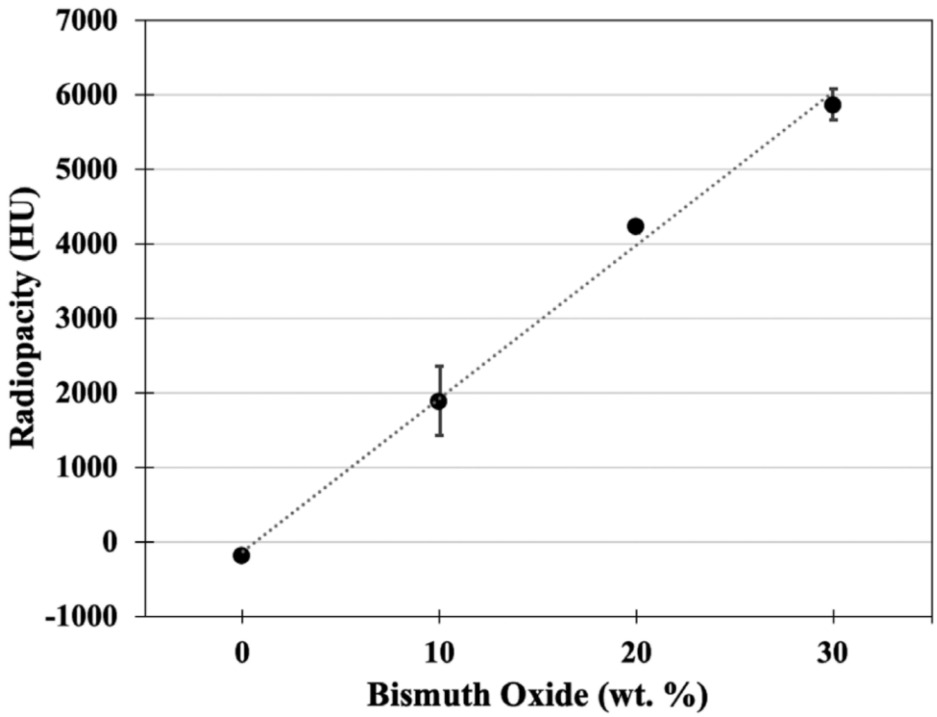

Figure 18: *Average CT number representing the radiopacity in Hounsfield units (HU) for varying concentrations of bismuth oxide in PLA. A linear fit (R2 = 0.99) to the data shows a change of approximately 196 HU with each percentage of additive. CT, computed tomography; PLA, polylactic acid*.

The average CT number of the printed cylindrical test specimens, based on five 2D slices of the 3D images of each concentration, is displayed in Figure 18. The CT number increased markedly with increasing Bi_2O_3 concentration. The average CT number of specimens containing 0, 10, 20, and 30 wt% concentrations was −22 ± 28, 2,487 ± 466, 4,218 ± 60, and 5,938 ± 208 HU, respectively. Based on a linear fit of the data (R2 = 0.99), the PLA contrast increased by approximately 196 HU with each weight percent of the Bi_2O_3 additive.

The linear fit in Figure 18 was used to estimate the additive concentration of an FFF filament that could provide radio-mimetic CT contrast of the spine phantom shown in Figure 14. A 1.5 wt% Bi_2O_3 contrast was predicted to yield a CT number of 508 ± 255 HU based on 95% confidence limits, which is within the reported range of cancellous and cortical bone (60).

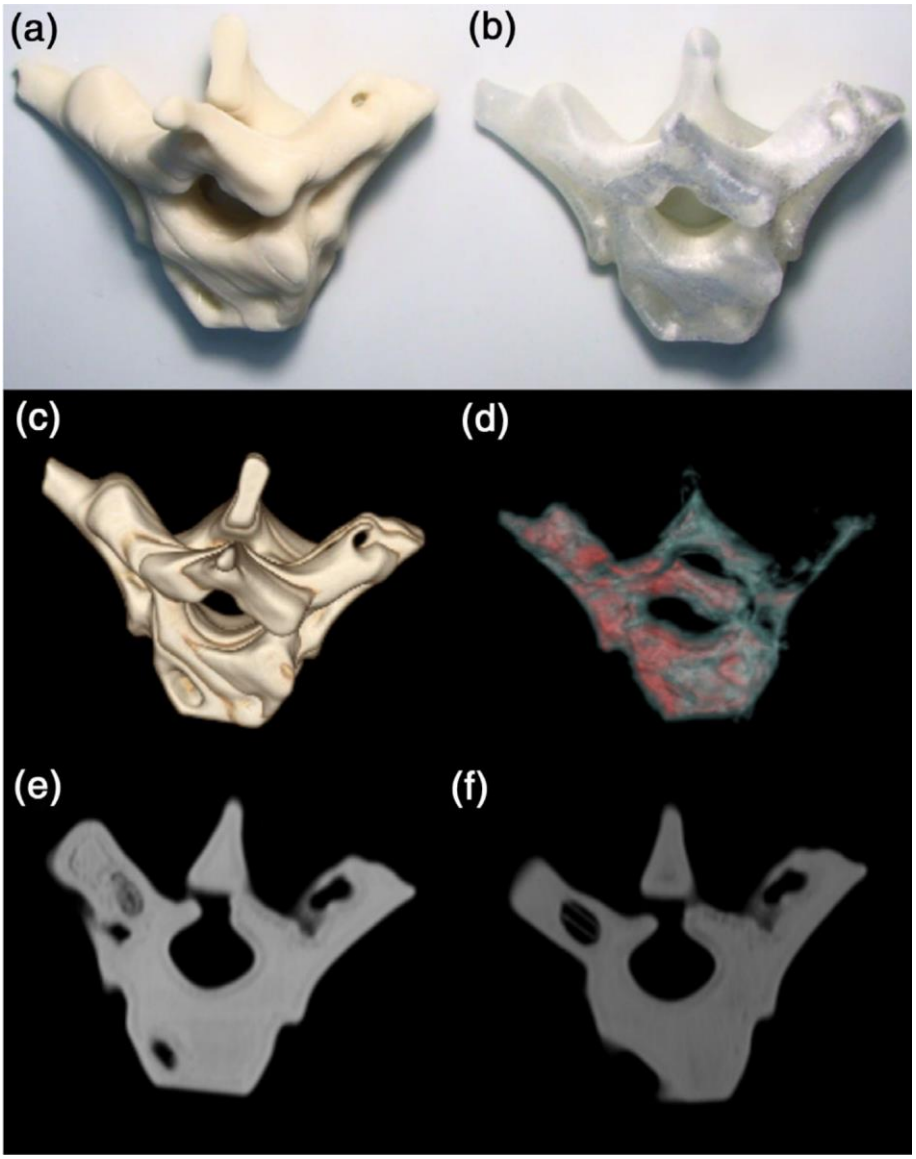

Figure 19: *Photos of a FFF printed phantom consisting of vertebral bodies containing (a) 1.5 and (b) 0.0 wt% bismuth oxide. 3D computed tomography (CT) images of the phantom are shown containing (c) 1.5 and (d) 0.0 wt% bismuth oxide and 2D CT images of the phantom containing (e) 1.5 and (f) 0.0 wt% bismuth oxide. FFF, fused filament fabrication.*

Figure 19a,b shows FFF prints of phantoms containing 1.5 wt and 0 wt% Bi_2O_3, respectively. The CT scans of the phantom containing Bi_2O_3 produced images that qualitatively look much more similar to bone (Figure 19c,e) compared to the PLA phantom with no additives (Figure 19d,f). The average CT number was determined from 25 random locations within the phantoms yielding a value of 119 ± 17 HU for the PLA phantom compared to 612 ± 87 HU for the phantom containing 1.5 wt% Bi_2O_3.

Further Discussion

The relatively minor change in the TG and TM of the composite granules produced in this study compared to pure PLA allowed for the use of FFF print bed and nozzle temperatures that are commonly used for PLA printing in commercial systems. While changes in the crystallinity behavior of PLA have been observed for several types of inorganic additives in other studies, the TG and TM often remain relatively unchanged and is consistent with the findings in this study (61, 62).

The representative stress–strain curves in Figure 15a shows a peak in stress followed by a downward slope prior to a sharp drop, indicative of specimen fracture. The downward slope in the curve occurs as fused layers within the specimens start to separate, which is commonly observed in FFF specimens with low porosity (63). The flat fracture surfaces of the tensile test specimens observed by SEM analysis is indicative of brittle fracture that is observed for semicrystalline polymers, such as PLA (28). The layered microstructure with interstitial voids is characteristic of the FFF printing process (14). This structure forms as the viscous filament is deposited, flows, and solidifies into a flattened morphology. The Bi_2O_3 particle agglomeration directly observed by SEM and micro-CT analysis increases as the additive concentration increases, which is expected at high additive loadings (19, 62). The micron-scale voids observed across the fracture surfaces of the tensile test specimens are likely due to pullout of the additives from the polymer upon fracture. An increase in agglomeration and poor interfacial adhesion between the Bi_2O_3 and the polymer results in an increase in stress concentrations throughout the material and is the likely cause for the reduction of strength observed at the 30 wt% concentration (64).

While a reduction of infill percentage of FFF prints often occurs due to interstitial void formation, the infill reduction could also be a result of an inconsistency of the extruded filament diameter leading to regions with under- and over-extrusion. The FFF system used in this study did not have a feedback system capable of modulating the filament feed rate based on changes in filament diameter, therefore some volumes likely received less material than specified. The measured diameter of the filaments produced in this study was 1.59 ± 0.34 mm. The relatively large diameter deviation was a result of the irregular shape of the composite granules which created voids within the screw extrusion process due to inconsistent packing in the feed hopper. This led to temporary increases and decreases in the filament extrusion rate. A more consistent diameter might be achieved by mixing the irregularly shaped granules with the more consistent PLA pellets for better packing and the use of vibration for better feeding of granules from the hopper. Though there was no major change in the TG and TM of the composites, an optimization of the extrusion temperature for each composite may also reduce the filament diameter variation.

The average radiopacity of the FFF printed test specimens and phantoms observed by micro-CT and CT increased with increasing Bi_2O_3 content due to an increase in the X-ray attenuation coefficient of the composite filament. Compared to a recent study using barium sulfate additives in FFF filaments, the Bi_2O_3 additive studied here provides approximately 24% higher radiopacity per wt%.22 Though some particle clustering was observed in the micro-CT images leading to a granular appearance of the composite, the cluster sizes were below the resolution of the CT system. Therefore, the printed spine phantom displayed a homogenous contrast throughout the filled volume. The calibration curve determined by micro-CT proved adequate to predict the Bi_2O_3 concentration required for the spine phantom to mimic the CT number of bone.

Conclusions

PLA filaments containing varying concentrations of Bi_2O_3 microparticle additives were created using solvent mixing, followed by drying, granulation, and extrusion. The composite filaments were produced with 0, 10, 20, and 30 wt% of the additives. Thermal analysis by DSC showed that only a moderate reduction of the TG and TM were observed, allowing the use of standard FFF printer settings for PLA.

Tensile mechanical testing was performed on FFF printed specimens to assess any change in mechanical behavior that could inhibit load-bearing applications. A slight decrease in the ultimate tensile strength of the printed specimens was observed only at the highest Bi_2O_3 concentrations studied. The modulus of the printed composite increased with each concentration of Bi_2O_3. The slight degradation of mechanical behavior was likely due to an increase of particle agglomerates as the concentration increased and stress concentrations formed. Particle agglomeration was confirmed in SEM images of the fracture surface of the test specimens and in micro-CT images of printed objects. While the mechanical strength of the printed objects was moderately reduced by the incorporation of the additive, this effect could likely be further reduced by the addition of surfactants to reduce agglomeration in the solvent processing stage. However, for the concentrations required for radio-mimetic biomedical phantoms, the observed reduction in mechanical strength is unlikely to reduce the materials applicability.

A linear increase in radiopacity was observed in micro-CT analysis of the printed test specimens. The radiopacity was observed to increase by 196 HU per wt% of bismuth oxide added. Based on these findings, a concentration of 1.5 wt% of Bi_2O_3 was used to print a spine phantom with a CT number that mimics the contrast of bone. Though some reduction in the infill of the printed composites was observed, these were below the resolution of typical medical CT systems. The Bi_2O_3-PLA composite had an average CT number of 612 ± 87 HU which is consistent with the typical range observed for cancellous and cortical bone.

This study shows that Bi_2O_3 is an effective additive in PLA filaments for mimicking the radiopacity of FFF printed biomedical bone phantoms. Compared to typical commercially available thermoplastic filaments, the radio-mimetic composites explored in this study are likely to provide greater efficacy for phantoms produced for preoperative preparation, resident training, and patient education.

Conclusion and Future Work

Conclusion

The composites investigated in both studies displayed the desired properties for which they were investigated. The AgSMW-PLA composite showed significant antibacterial activity at 10 %wt particle loading. At this concentration bacterial growth was reduced by nearly 50%. The Bi_2O_3-PLA composite displayed x-ray absorptive properties at all particle loadings tested. The x-ray absorption of the composite material increased linearly with increased particle loading.

With the exception of the production of the particle additives and the testing performed to assess the extent to which the desired properties were achieved, the AgSMW study and the Bi_2O_3 study were quite similar in their methodology. Both studies utilized the same techniques to produce the particle-PLA composite filament, the same method to assess changes in thermal behavior, and the same procedures for producing and testing tensile specimens. The specifics of these similarities have been previously discussed in *Introduction,* and in *Processing, Characterization, and Testing*.

The two studies were also broadly similar in the results of both DSC and tensile testing. Both composite materials displayed similar changes in thermal behavior and mechanical properties with increased particle loading. A direct comparison is not possible due to the differing increments of particle loading selected in each study, the AgSMW study used a logarithmic increment while the Bi_2O_3 study used a linear increment. Even so, a similar trend can be observed in the mechanical and thermal properties of both composites. The glass transition temperature and the melting point of both composites was slightly reduced compared to pure PLA. As particle loading increases, ultimate strength decreases and modulus increases. These results agree with expectations based on previous studies of microparticle-polymer composites (19, 25, 26, 27, 29).

Future Work

The AgSMW study used a logarithmic increment to determine the particle loadings tested. This was done due to the time-consuming synthesis required to produce the particles. Unfortunately, it left quite a large gap between the 1 %wt particle loading, where negligible antibacterial activity was observed, and 10 %wt particle loading, where significant antibacterial activity was observed. A future study investigating AgSMW-PLA composites at particle loadings between 1 wt% and 10 wt% would be beneficial to determine the required particle loading to achieve useful antimicrobial activity.

SEM analysis of the fracture surfaces indicated insufficient bonding between the AgSMW particles and the surrounding polymer. A future study investigating the use of particle coatings other than PVP would be useful to determine if better particle-polymer binding can be achieved.

While the result of the Bi_2O_3 study showing a linear increase in x-ray absorption with increased particle loading is useful, most FFF printers use a single spool of filament. This may make using the Bi_2O_3-PLA composite to mimic the varying x-ray absorption of different areas within the same bone somewhat cumbersome. A future study investigating whether this varying x-ray absorption can be mimicked by altering the infill settings of the FFF printer, while using a filament of only one particle loading, would be beneficial.

References

1. Advanced Secondary Fuel Nozzle Upgrade | GE Gas Power. (n.d.). Gepower-V2. Retrieved October 23, 2023, from https://www.ge.com/gas-power/services/gas-turbines/upgrades/advanced-secondary-fuel-nozzle

2. Orme, M. (2022.). How AM is Disrupting the Aerospace Industry. www.sme.org. https://www.sme.org/technologies/articles/2022/may/how-am-is-disrupting-the-aerospace-industry/

3. Scopigno R., Cignoni P., Pietroni N., Callieri M., Dellepiane M. (2017). "Digital Fabrication Techniques for Cultural Heritage: A Survey". *Computer Graphics Forum* 36 (1): 6–21. DOI:10.1111/cgf.12781

4. Auras R, Lim LT, Selke SE, Tsuji H, eds. (2010). Poly(Lactic Acid): Synthesis, Structures, Properties, Processing, and Applications. doi:10.1002/9780470649848. ISBN 978-0-470-29366-9.

5. Dul, S., Fambri, L. and Pegoretti, A. (2016), "Fused deposition modeling with ABS-Graphene nanocomposites", Composites Part A: Applied Science and Manufacturing, Vol. 85, pp. 181-191.

6. Wu, W., Geng, P., Li, G., Zhao, D., Zhang, H. and Zhao, J. (2015), "Influence of layer thickness and raster angle on the mechanical properties of 3D-printed PEEK and a comparative mechanical study between PEEK and ABS", Materials, Vol. 8 No. 9, pp. 5834-5846.

7. Yang, C., Tian, X., Liu, T., Cao, Y. and Li, D. (2017), "3D printing for continuous fiber reinforced thermoplastic composites: mechanism and performance", Rapid Prototyping Journal, Vol. 23 No. 1, pp. 209-215.

8. Perez, A.R.T., Roberson, D.A. and Wicker, R.B. (2014), "3D printing for continuous fiber reinforced thermoplastic composites: mechanism and performance", Journal of Failure Analysis and Prevention, Vol. 14, pp. 343-352.

9. Society of Manufacturing Engineers (SME) Annual Report (2018), "Medical additive manufacturing/3D printing", available at: www.sme.org (accessed 30 March 2019).

10. Jin, Y.-A., Plott, J., Chen, R., Wensman, J. and Shih, A. (2015), "Additive manufacturing of custom orthoses and prostheses - a review", Procedia CIRP, Vol. 36, pp. 199-204.

11. Centers for Disease Control and Prevention (2017), "Current HAI progress report", available at: www.cdc.gov/hai/data/ portal/progress-report.html(accessed 30 March 2019).

12. Cloutier, M., Mantovani, D. and Rosei, F. (2015), "Antibacterial coatings: challenges, perspectives, and opportunities", Trends in Biotechnology, Vol. 33 No. 11, pp. 637-652.

13. Page, K., Wilson, M. and Parkin, I.P. (2009), “Antimicrobial surfaces and their potential in reducing the role of the inanimate environment in the incidence of Hospital Acquired infections”, Journal of Materials Chemistry, Vol. 23, pp. 3819-3831.

14. Gibson, I., Rosen, D. and Stucker, B. (2015), Additive Manufacturing Technologies, Springer, New York, NY.

15. LeOuay, B. and Stellacci, F. (2015), “Antibacterial activity of silver nanoparticles: a surface science insight”, Nano Today, Vol. 10, pp. 339-354.

16. Palza, H., Quijada, R. and Delgado, K. (2015), “Antimicrobial polymer composites with copper micro- and nanoparticles: effect of particle size and polymer matrix”, Journal of Bioactive and Compatible Polymers, Vol. 30 No. 4, pp. 1-15.

17. Chernousova, S. and Epple, M. (2015), “Silver as antibacterial agent: ion, nanoparticle, and metal”, Angewandte Chemie (International ed. In English), Vol. 52 No. 6, pp. 1636-1653.

18. Saini, P., Arora, M. and Kumar, M.N.V.R. (2016), “Poly (lactic acid) blends in biomedical applications”, Advanced Drug Delivery Reviews, Vol. 107, pp. 47-59.

19. Blattmann, C.O. and Pratsinis, S.E. (2016), “Nanoparticle filler content and shape in polymer nanocomposites”, Kona Powder and Particle Journal, Vol. 36 No. 1, pp. 1-30.

20. Doganay, D., Coskun, S., Kaynak, C. and Unalan, H.E. (2016), “Electrical, mechanical and thermal properties of aligned silver nanowire/polylactide nanocomposite films”, Composites Part B: Engineering, Vol. 99, pp. 288-296.

21. Hussain, S.M., Braydich-Stolle, L.K., Schrand, A.M., Murdock, R.C., Yu, K.O., Mattie, D.M., Schlager, J.J. and Terrones, M. (2009), “Toxicity evaluation for safe use of nanomaterials: recent achievements and technical challenges”, Advanced Materials, Vol. 21 No. 16, pp. 1549-1559.

22. Müller, K., Bugnicourt, E., Latorre, M., Jorda, M., Sanz, Y.E., Lagaron, J.M., Miesbauer, O., Bianchin, A., Hankin, S., Bölz, U., Pérez, G., Jesdinszki, M., Lindner, M., Scheuerer, Z., Castello. and Schmid, M. (2017), “Review on the processing and properties of polymer nanocomposites and nanocoatings and their applications in the packaging, automotive and solar energy fields”, Nanomaterials, Vol. 7 No. 4, pp. 1-47.

23. Wiley, B., Sun, Y., Mayers, B. and Xia, Y. (2005), “Shape control of silver nanoparticles”, Chemistry (Weinheim an Der Bergstrasse, Germany), Vol. 11 No. 2, pp. 454-463.

24. Sun, Y. and Xia, Y. (2002), “Shape-control synthesis of gold and silver nanoparticles”, Science, Vol. 298 No. 5601, pp. 2176-2179.

25. Fortunati, E., Armentano, I., Zhou, Q., Puglia, D., Terenzi, A., Berglund, L.A. and Kenny, J.M. (2012), “Microstructure and nonisothermal cold crystallization of PLA composites based on silver nanoparticles and nanocrystalline cellulose”, Polymer Degradation and Stability, Vol. 97 No. 10, pp. 2027-2036.

26. Fortunati, E., Armentano, I., Zhou, Q., Iannoni, A., Saino, E., Visai, L., Berglund, L.A. and Kenny, J.M. (2012), "Multifunctional bionanocomposite films of poly(lactic acid), cellulose nanocrystals and silver nanoparticles", Carbohydrate Polymers, Vol. 87 No. 2, pp. 1596-1605.

27. Rhim, J.W., Mohanty, A.K., Singh, S.P. and Ng, P.K.W. (2006), "Effect of the processing methods on the performance of polylactide films: thermocompression versus solvent casting", Journal of Applied Polymer Science, Vol. 101 No. 6, pp. 3736-3742.

28. Kinloch, A.J. and Young, R.J. (1995), Fracture Behaviour of Polymers, Springer, New York, NY.

29. Khaliq, M.H., Gomes, R., Fernandes, C., Nobrega, J.M., Carneiro, O.S. and Férras, L.L. (2017), "On the use of high viscosity polymers in the fused filament fabrication process", Rapid Prototyping Journal, Vol. 23 No. 4, pp. 727-735.

30. Costa, A.E., Ferreira da Silva, A. and Carneiro, O.S. (2018), "A study on extruded filament bonding in fused filament fabrication", Rapid Prototyping Journal, Vol. 25 No. 3, pp. 555-565.

31. Kalathi, J.T., Grest, G.S. and Kumar, S.K. (2012), "Universal viscosity behavior of polymer nanocomposites", Physical Review Letters, Vol. 109 No. 19, p. 198301.

32. Damm, C., Munstedt, H. and Rosch, A. (2008), "The antimicrobial efficacy of polyamide 6/Silver-Nano- and microcomposites", Materials Chemistry and Physics, Vol. 108 No. 1, pp. 61-66.

33. Ton-That, T.M. and Jungnickel, B.J. (1999), "Water diffusion into transcrystalline layers on polypropylene", Journal of Applied Polymer Science, Vol. 74 No. 13, pp. 3275-3285.

34. Cioffi, N., Torsi, L., Ditarantano, N., Tantalillo, G., Ghibelli, L., Sabbatini, L., Bleve-Zacheo, T., D'Alessio, M., Zambonin, P.G. and Traversa, E. (2005), "Copper nanoparticle/polymer composites with antifungal and bacteriostatic properties", Chemistry of Materials, Vol. 17 No. 21, pp. 5255-5262.

35. Yew, G.H., Yusof, A.M.M., Ishak, Z.A.M. and Ishiaku, U.S. (2005), "Water absorption and enzymatic degradation of poly(lactic acid)/rice starch composites", Polymer Degradation and Stability, Vol. 90 No. 3, pp. 488-500.

36. Kalaskar DM, ed. 3D printing in medicine. Duxford Cambridge, MA Kidlington: WP, Woodhead Publishing, an imprint of Elsevier; 2017:226.

37. Haleem A, Mohd J. 3D scanning applications in medical field: a literature-based review. Clin Epidemiol Global Health. 2019;7:199-210.

38. Mohd J, Haleem A. Additive manufacturing applications in medical cases: a literature based review. Alexandria J Med. 2018;54: 411-422.

39. Zuniga J. 3D printed antibacterial prostheses. Appl Sci. 2018;8:1651.

40. Witowski JS, Coles-Black J, Zuzak TZ, et al. 3D printing in liver surgery: a systematic review. Telemed J E Health. 2017;23:943-947.

41. Rui Y, Gang X, Shuang-Shuang M, et al. Three-dimensional printing: review of application in medicine and hepatic surgery. Cancer Biol Med. 2016;13:443-451.

42. Garcia J, Yang Z, Mongrain R, Leask RL, Lachapelle K. 3D printing materials and their use in medical education: a review of current technology and trends for the future. BMJ Simul Technol Enhanc Learn. 2018;4:27-40.

43. Wang K, Ho C-C, Zhang C, Wang B. A review on the 3D printing of functional structures for medical phantoms and regenerated tissue and organ applications. Engineering. 2017;3:653-662.

44. O'Reilly MK, Reese S, Herlihy T, et al. Fabrication and assessment of 3D printed anatomical models of the lower limb for anatomical teaching and femoral vessel access training in medicine: subject specific 3D-printed anatomy. Am Assoc Anatomists. 2016;9:71-79.

45. Langridge B, Momin S, Coumbe B, Woin E, Griffin M, Butler P. Systematic review of the use of 3-dimensional printing in surgical teaching and assessment. J Surg Educ. 2018;75:209-221.

46. Li KHC, Kui C, Lee EKM, Ho CS, Sunny Hei SH, Wu W, Wong WT, Voll J, Li G, Liu T, Yan B, Chan J, Tse G, Keenan ID. The role of 3D printing in anatomy education and surgical training: a narrative review. MedEdPublish [Internet]. [cited 2020 Mar 7] 2017;6(2):6. Available from: *https://www.mededpublish.org/manuscripts/1010/v1*

47. Lichtenberger JP, Tatum PS, Gada S, Wyn M, Ho VB, Liacouras P. Using 3D printing (additive manufacturing) to produce low-cost simulation models for medical training. Mil Med. 2018;183:73-77.

48. Pucci JU, Christophe BR, Sisti JA, Connolly ES. Three-dimensional printing: technologies, applications, and limitations in neurosurgery. Biotechnol Adv. 2017;35:521-529.

49. Randazzo M, Pisapia J, Singh N, Thawani J. 3D printing in neurosurgery: a systematic review. Surg Neurol Int. 2016;7:801.

50. Chen C, Cai L, Zheng W, Wang J, Guo X, Chen H. The efficacy of using 3D printing models in the treatment of fractures: a randomised clinical trial. BMC Musculoskelet Disord. 2019;20:65.

51. Coote JD, Nguyen T, Tholen K, et al. Three-dimensional printed patient models for complex pediatric spinal surgery. Ochsner J. 2019; 19:49-53.

52. Luu K, Pakdel A, Wang E, Prisman E. In house virtual surgery and 3D complex head and neck reconstruction. J Otolaryngol Head Neck Surg. 2018;47:75.

53. Smelt JLC, Suri T, Valencia O, et al. Operative planning in thoracic surgery: a pilot study comparing imaging techniques and three-dimensional printing. Ann Thorac Surg. 2019;107:401-406.

54. Thompson A, McNally D, Maskery I, Leach RK. X-ray computed tomography and additive manufacturing in medicine: a review. Int J Metrol Qual Eng. 2017;8:17.

55. Ceh J, Youd T, Mastrovich Z, et al. Bismuth infusion of ABS enables additive manufacturing of complex radiological phantoms and shielding equipment. Sensors. 2017;17:459.

56. Hamedani BA, Melvin A, Vaheesan K, Gadani S, Pereira K, Hall AF. Three-dimensional printing CT-derived objects with controllable radiopacity. J Appl Clin Med Phys. 2018;19:317-328.

57. Garcea SC, Wang Y, Withers PJ. X-ray computed tomography of polymer composites. Compos Sci Technol. 2018;156:305-319.

58. Mottu F, Rüfenacht DA, Doelker E. Radiopaque polymeric materials for medical applications: current aspects of biomaterial research. Invest. Radiol. 1999;34:323-335.

59. Mah P, Reeves TE, McDavid WD. Deriving Hounsfield units using grey levels in cone beam computed tomography. Dentomaxillofac Radiol. 2010;39:323-335.

60. Patrick S, Np B, Gurushanth K, As R, Gurudath S. Comparison of gray values of cone-beam computed tomography with hounsfield units of multislice computed tomography: an in vitro study. Indian J Dent Res. 2017;28:66.

61. Chu Z, Zhao T, Li L, Fan J, Qin Y. Characterization of antimicrobial poly (lactic acid)/Nano-composite films with silver and zinc oxide nanoparticles. Materials. 2017;10:659.

62. Walker JS, Arnold J, Shrestha C, Smith D. Antibacterial silver submicron wire-polylactic acid composites for fused filament fabrication. Rapid Prototyping J. 2020;26:32-38.

63. Zhang HY, Jiang HB, Ryu J-H, Kang H, Kim K-M, Kwon J-S. Comparing properties of variable pore-sized 3D-printed PLA membrane with conventional PLA membrane for guided bone/tissue regeneration. Materials. 2019;12:17-18

64. Budynas RG, Nisbett JK, Shigley JE. Shigley's mechanical engineering design. Eleventh ed. New York, NY: McGraw-Hill Education; 2020. 40. Dizon JRC, Espera AH, Chen Q, Advincula RC. Mechanical characterization of 3D-printed polymers. Addit Manuf. 2018;20:44-67.

Vita

The author was born in Metairie, Louisiana. He joined Professor Damon Smith's research lab, part of the Advanced Materials Research Institute at the University of New Orleans, as an undergraduate student in 2017. After obtaining his Bachelor of Science degree in Mechanical Engineering from The University of New Orleans in 2018, he remained in the Mechanical Engineering department as a Research and Teaching assistant pursuing a Master of Science in Engineering degree with a concentration in Mechanical Engineering.